Fracture of vacancy-defected carbon nanotubes and their embedded nanocomposites

Shaoping Xiao and Wenyi Hou
Department of Mechanical and Industrial Engineering, and Center for Computer-Aided Design, The University of Iowa, Iowa City, Iowa 52242, USA

(Received 11 December 2005; revised manuscript received 17 January 2006; published 8 March 2006)

In this paper, we investigate effects of vacancy defects on fracture of carbon nanotubes and carbon nanotube/aluminum composites. Our studies show that even a one-atom vacancy defect can dramatically reduce the failure stresses and strains of carbon nanotubes. Consequently, nanocomposites, in which vacancy-defected nanotubes are embedded, exhibit different characteristics from those in which pristine nanotubes are embedded. It has been found that defected nanotubes with a small volume fraction cannot reinforce but instead weaken nanocomposite materials. Although a large volume fraction of defected nanotubes can slightly increase the failure stresses of nanocomposites, the failure strains of nanocomposites are always decreased.

DOI: 10.1103/PhysRevB.73.115406 PACS number(s): 61.46.Fg, 81.05.Ni

I. INTRODUCTION

It is known that carbon nanotubes (CNTs) have large tensile modulus[1,2] and high thermal conductivity.[3,4] The Young's moduli of CNTs are around 1 Tpa and their thermal conductivity can be 6600 W/m K. On the other hand, CNTs are expected to have high strength. Previous theoretical analyses and numerical simulations predicted failure strengths of up to 300 Gpa for CNTs.[5–7] Consequently, they have been proposed as ideal fibers for the manufacture of the next generation of composite materials with mechanical and thermal management applications.[8–10] However, low failure stresses, which are in the range of 21–63 Gpa, were observed in the experiments.[11] Such observation conflicted with theoretical and numerical analyses outcomes.

Some researchers have pointed out the significant effects of defects on nanotube fracture.[12,13] Defects in CNTs can arise from various causes. Chemical defects consist of atoms/groups covalently attached to the carbon lattice of the tubes such as oxidized carbon sites or chemical vapor deposition.[14,15] Topological defects correspond to the presence of rings other than hexagons, mainly studied as pentagon/heptagon pairs.[16,17] Incomplete bonding defects like vacancies may be caused through impact with high-energy electrons in the transmission electron microscopy environment, see Banhart,[18] or defects in the original outer nanotube shell.

Chemical defects usually occur during functionalizing CNTs so that chemical bonds can be formed between CNTs and the matrix material in nanocomposites. Consequently, the mechanical properties of nanocomposites can be significantly enhanced[19,20] because of the strong interfacial load transfer. However, we do not think that functionalization will have significant effects on the nanotube fracture itself. 5/7/7/5 dislocation, also called Stone-Wales dislocation, results in high failure strengths[5,7] in comparison with the experimental results. Incomplete bonding, especially vacancy, will form nanoscale cracks or holes that can have large variations in size. Such an initial mechanism can dramatically reduce the strength of CNTs. Belytschko *et al.*[12] obtained reasonable results that can account for the fractures in the experiments[11] with an n-atom defect model (vacancy due to n atoms missing). However, since the bonds along the hypothetical crack were not reconstructed, the physical plausibility of these defects remains in question. In research performed in collaboration with Belytschko, Car, Ruoff, Schatz, etc., the role of vacancy defects and holes in the fracture of CNTs[13] was studied. Both quantum mechanical and molecular mechanics calculations indicated that the holes due to one- and two-atom vacancy defects could reduce failure stresses by as much as ~26%. In their studies, nanotubes were assumed at zero temperature.

Since high strengths of CNTs were predicted, it was assumed that the toughness of their embedded composite materials could be significantly increased.[19–21] Generally, three types of materials can be used as the matrix: polymers,[21,22] ceramics,[23,24] and metal.[25,26]. Because polymers have low density and are easy to shape, they are the first choice as the matrix of fiber reinforced composites. As a structural material, ceramics present many advantages over polymers, such as high rigidity and hardness, even at high temperature, and low sensitivity to corrosion. However, they are brittle. Such weakness can be made up by reinforcing the composites with CNTs. Lately, there has been more interest in using metal as the matrix material for composites. It has been found that the fracture toughness of a metal matrix composite with nanotubes can be increased by up to 200%.[27]

In this paper, we will first study the failure mechanism of vacancy-defected CNTs using molecular dynamics. As a difference from previous research work, vacancy defects are modeled by taking out atoms and then reconstructing bonds. Various temperatures will be considered to investigate temperature effects on the fracture of CNTs. We also study size effects of vacancy defects on a nanotube fracture at room temperature, i.e., T=300 K. Then, nanotube-embedded aluminum (CNT/Al) composites are considered to investigate effects of vacancy defects on fracture of nanocomposites. In this paper, only nonbonded interatomic interaction, i.e., van der Waals energy, is considered at the CNT/Al interface, since no chemical reactions were observed during processing of CNT/Al composites in the experimentation.[27]

II. COMPUTATIONAL MODELS

A. Molecular dynamics

In molecular dynamics simulations, the following equations of motion are solved for the whole simulated system without the consideration of external forces:

$$m_I \ddot{\mathbf{d}}_I = -\frac{\partial E}{\partial \mathbf{x}_I} \tag{1}$$

where m_I is the mass of atom I, $\mathbf{x}_I$ is its position, and $\mathbf{x}_I = \mathbf{X}_I + \mathbf{d}_I$ ($\mathbf{X}_I$ is the original position of atom I and $\mathbf{d}_I$ is its displacement). $E(\mathbf{x})$ is the potential function. A Hoover thermostat[28] is implemented so a constant temperature can be maintained during molecular dynamics simulations.

B. Carbon nanotubes

In this paper, only single-walled carbon nanotubes (SWNTs) are considered. The modified Morse potential function[7] is employed to describe interatomic interaction in carbon nanotubes. This potential can be written as

$$E = E_{\text{stretch}} + E_{\text{angle}},$$

$$E_{\text{stretch}} = D_e\{[1 - e^{-\beta(r-r_0)}]^2 - 1\},$$

$$E_{\text{angle}} = \frac{1}{2}k_\theta(\theta - \theta_0)^2[1 + k_s(\theta - \theta_0)^4], \tag{2}$$

where E_{stretch} is the bond energy due to bond stretching or compressing, E_{angle} is the bond energy due to bond angle-bending, r is the current bond length, and θ is the angle of two adjacent bonds representing a standard deformation measure in molecular mechanics. The parameters are

$$r_0 = 1.42 \times 10^{-10}\ \text{m}, \quad D_e = 6.03105 \times 10^{-19}\ \text{N m},$$

$$\beta = 2.625 \times 10^{10}\ \text{m}^{-1}, \quad \theta_0 = 2.094\ \text{rad},$$

$$k_\theta = 1.13 \times 10^{-18}\ \text{N m/rad}^2, \quad k_s = 0.754\ \text{rad}^{-4}. \tag{3}$$

It has been shown that this potential function results in reasonable Young's modulus and Poisson's ratio of nanotubes compared with experimental investigations. Belytschko and his co- workers[7] showed that the modified Morse potential could predict nanotube fracture better than the Brenner's potential.[29]

Before molecular dynamics simulation, the equilibrium state of nanotubes needs to be obtained via energy minimization. During the simulation, one end of the tubes is fixed and another end is loaded with prescribed displacements. For each displacement increment, 0.005 nm, the tube was equilibrated for 1000 time steps. Another 100 time steps are used to calculate the time-averaged external force F. The applied external force F can be calculated by summing the internal forces applied on the prescribed displaced atoms. One can obtain the stress via $\sigma = F/(\pi D h)$, where D is the tube diameter and h is the tube thickness, i.e., 0.34 nm.

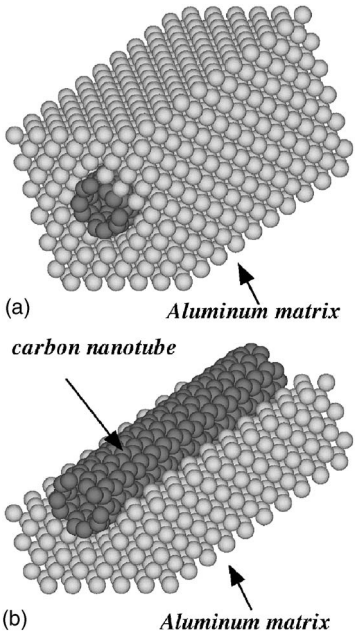

FIG. 1. CNT-embedded aluminum composites.

C. CNT/Al composites

The unit cell model of nanotube-embedded aluminum composites is shown in Fig. 1 in that only long continuous tubes are considered. We also assume that the nanotubes are homogeneously distributed with uniaxial alignment. Periodic boundary conditions are employed. The total potential of the simulated CNT/Al composite cell can be written as

$$E = E_{\text{CNT}} + E_{\text{Al}} + E_{\text{LJ}} \tag{4}$$

where E_{CNT} is the potential of the embedded carbon nanotube and is calculated from Eq. (2). An embedded-atom method potential function[30,31] is used for Al–Al bonds and it is

$$E_{\text{AL}} = \frac{1}{2}\sum_{ij} V(r_{ij}) + \sum_i F(\overline{\rho}_i), \tag{5}$$

where $V(r_{ij})$ is a pairwise potential as a function of distance between atom i and atom j, and F is the "embedding energy" as a function of the "atomic density" $\overline{\rho}_i$ that represents environment effects by all surrounding atoms in the system. The latter is given by

$$\overline{\rho}_i = \sum_{j \neq i} \rho(r_i) \tag{6}$$

where $\rho(r_{ij})$ is the "atomic density" function.

Since only weak CNT/Al interfaces were observed in the experimentation,[27] the Lennard-Jones potential as follows is used to describe nonbonded interaction between the embedded carbon nanotube and the aluminum matrix.

$$E_{\text{LJ}} = 4\varepsilon\left[\left(\frac{\sigma}{r}\right)^{12} - \left(\frac{\sigma}{r}\right)^{6}\right]. \tag{7}$$

The parameters for the interactions between carbon atoms and aluminum atoms are obtained from the Lorentz-Berelot

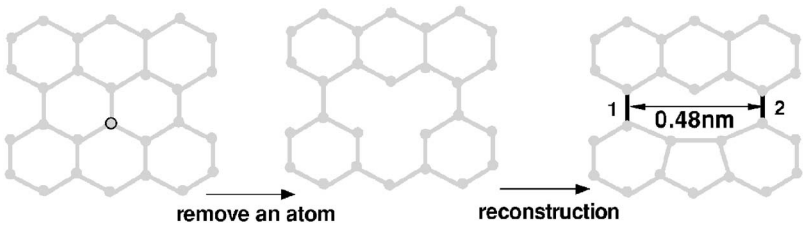

FIG. 2. One-atom vacancy defect in a zigzag nanotube.

combining rules: $\varepsilon=0.038$ eV and $\sigma=0.296$ nm. The simulation procedure is similar to what is described above.

III. FRACTURE OF VACANCY-DEFECTED NANOTUBES

In this paper, we assume that vacancy defects are present in the middle of nanotubes. The vacancy defects are modeled by taking out atoms and then reconstructing bonds. If a single atom is removed from a zigzag tube, a 12-membered ring exists. Such a ring can be reconstructed to a pentagon and an enneagon as shown in Fig. 2. This configuration is identical to the symmetric configuration defined in Ref. 13. Although there are other possible configurations,[13] the asymmetric configurations, during the reconstruction, we use the symmetric one because it results in a lower potential for a one-atom vacancy-defected nanotube than asymmetric configurations. When such a nanotube is under tension, bond 1 and 2 of the enneagon will become unstable and broken first. Then, the crack will propagate along the circumference of the tube until the tube is broken.[32] The one-atom vacancy-defected nanotube, shown in Fig. 2, can be viewed as the nanotube containing an initial crack. The crack length, which is the distance between bonds 1 and 2, is 0.48 nm. Here, we neglect the curvature effect of nanotubes.

If a zigzag nanotube contains a two-atom vacancy defect, a bond will be removed and a crack will be initiated after bond reconstruction. In this paper, we assume the initial crack is always perpendicular to the tube axis to simplify the model. The configuration of a two-atom vacancy defect as shown in Fig. 3(a) is the most possible configuration because it requires less energy to remove a bond than two separated atoms. It can be seen that the initial crack length is equal to the length in a one-atom vacancy-defected tube as shown in Fig. 2. Similarly, Fig. 3(b) shows a four-atom vacancy defect, in which an initial crack of 0.73 nm exists after taking out two bonds. For armchair nanotubes, one-atom, two-atom (one-bond), and four-atom (two-bond) vacancies will result in initial cracks with lengths of 0.21, 0.28, and 0.49 nm, respectively, as shown in Fig. 4. Models for longer initial cracks can be generated similarly for both zigzag and armchair nanotubes.

We first investigate the fracture of (40,0) zigzag nanotubes containing one-atom, two-atom, and four-atom vacancy defects separately. All the nanotubes have a length of 6.0 nm and a radius of 1.5 nm. Various temperatures are considered. Figure 5 illustrates that the calculated failure stresses and strains of defected nanotubes are compared with those of the pristine (40,0) nanotube. It can be seen that higher temperatures result in lower failure stresses and strains. However, the temperature effects on fracture of vacancy-defected nanotubes are not as significant as those effects on fracture of pristine nanotubes. Figure 5(a) shows that the strength of the pristine (40,0) zigzag nanotube at 2000 K is reduced by 23% compared with its strength at 0 K. However, for defected zigzag nanotubes, the strengths are reduced only by 15%. It also can be seen that failure stresses and strains for one-atom and two-atom vacancy-defected zigzag nanotubes are similar because the lengths of the initial cracks are the same [see Figs. 2 and 3(a)].

As well, we study the size effect of vacancy defects on a nanotube fracture at the room temperature of 300 K. Initial cracks with various lengths up to 2 nm are considered. Figure 6 compares failure stresses of (40,0) vacancy-defected zigzag nanotubes and those of (23,23) vacancy-defected armchair nanotubes. Both (40,0) zigzag nanotubes and (23,23) armchair nanotubes have a similar length and diameter. We can see that the pristine armchair nanotube has a higher failure stress than the pristine zigzag nanotube. Belytschko and his co-workers[7] also gave the same conclusion. Furthermore, vacancy-defected armchair nanotubes have higher failure stresses than vacancy-defected zigzag nanotubes if the initial crack lengths are the same. The exception is that when the initial crack length is 0.48 nm, failure stresses are the same for both armchair and zigzag tubes. Such a phenomenon can be observed at various temperatures, as the failure stresses listed in Table I show.

We think this phenomenon is due to different fracture models occurring in different nanotubes. For a zigzag nano-

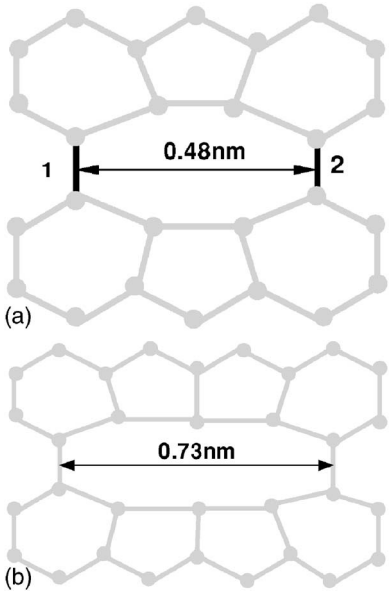

FIG. 3. Initial cracks in zigzag nanotubes. (a) Two-atom vacancy and (b) four-atom vacancy.

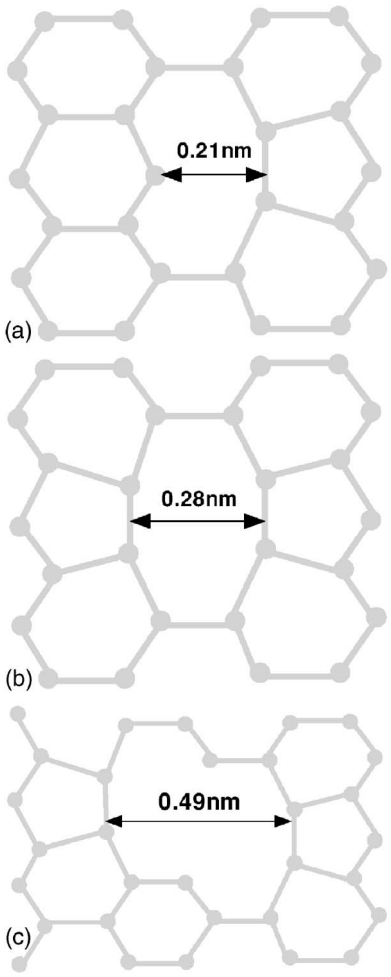

FIG. 4. Initial cracks in armchair nanotubes. (a) One-atom vacancy, (b) two-atom vacancy and (c) four-atom vacancy.

tube, the crack propagates along its circumference until it is broken. The fracture is mode I fracture as shown in Fig. 7(a). For an armchair tube with an initial crack of length 0.48 nm, a mode I fracture is mainly observed [see Fig. 7(b)] so that the failure stress is similar to that of a zigzag tube containing the initial crack with the same length. For other vacancy-defected armchair nanotubes, cracks propagate along the angle of 30° with the axis of the tube due to the geometry of an armchair tube, as the example shown in Fig. 7(c). Therefore a mixed mode I/II fracture occurs and the calculated failure stresses are higher than those of zigzag nanotubes containing initial cracks with the same length.

From Fig. 6 we also can see that the vacancy-defected zigzag tubes with longer initial cracks up to 1.0 nm have lower failure stresses. When the length of an initial crack is

TABLE I. Comparison of failure stresses (GPa) of nanotubes with a 0.48-nm-long initial crack at various temperatures

	10 K	300 K	600 K	1000 K
(40,0) zigzag nanotube	64.82	62.22	60.54	57.90
(23,23) armchair nanotube	64.56	61.43	60.54	57.41

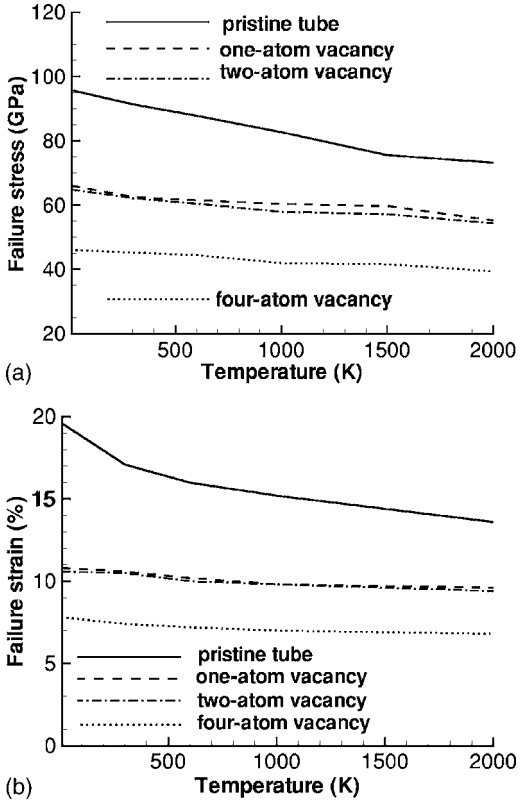

FIG. 5. Fracture of (40,0) zigzag nanotubes at various temperatures: (a) failure stresses and (b) failure strains.

larger than 1.0 nm, size effects of initial cracks on zigzag nanotube fracture are not significant. Therefore, a length of 1.0 nm can be viewed as the critical length for size effects of initial cracks on zigzag nanotube fracture. Such a critical initial crack length for armchair nanotubes is 1.4 nm as illustrated in Fig. 6. It should be noted that the initial crack lengths are fairly small compared to the circumference length of nanotubes. Therefore, size effects of nanotubes are ignored.

IV. FRACTURE OF CNT/Al NANOCOMPOSITES

In this paper, we also investigate aluminum-based nanocomposites in that long continuous carbon nanotubes are embedded with uniform alignment and homogeneous distribu-

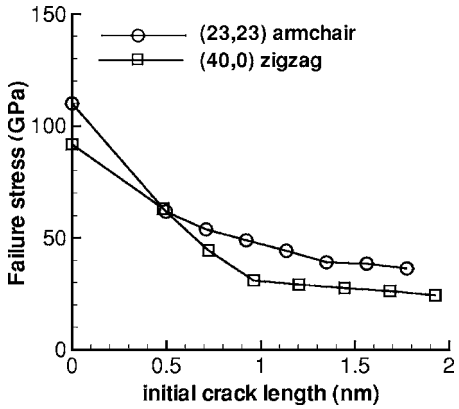

FIG. 6. Failure stresses of defected nanotubes at 300 K.

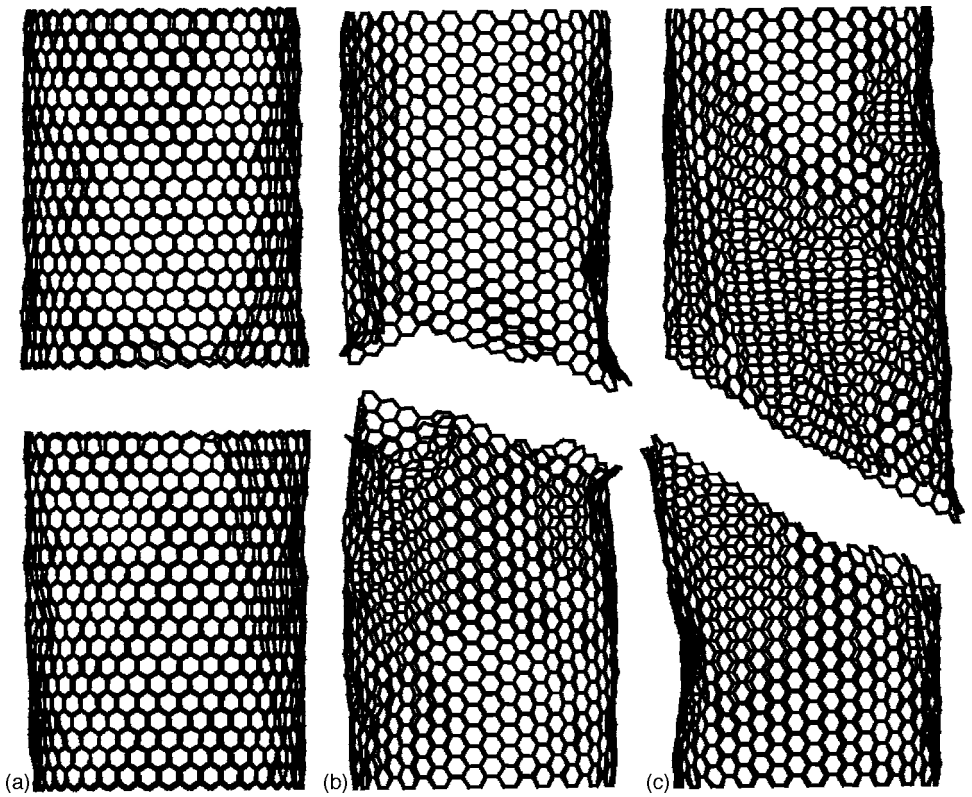

FIG. 7. Fracture modes of (a) a (40,0) zigzag nanotube with an initial crack of length 0.48 nm (mode I fracture); (b) a (23,23) armchair nanotube with an initial crack of length 0.48 nm (mode I fracture); and (c) a (23,23) armchair nanotube with an initial crack of length 0.92 nm (mixed mode I/II fracture).

tion. A unit cell model of aluminum nanocomposites with periodic boundary conditions is studied as illustrated in Fig. 1. We first consider the unit cell with the following dimensions: length of 2.16 nm, width of 2.16 nm, and depth of 4.32 nm. (5,5) armchair nanotubes, which have a diameter of 0.679 nm and a length of 4.32 nm, are embedded in the composite materials. Consequently, there are a total of 1712 aluminum atoms and 320 carbon atoms. The volume fraction of a carbon nanotube in the nanocomposite is 20%. The prescribed displacement is applied along the axial direction of the nanotube to investigate fracture of nanocomposites. Both the pristine tube and the defected tube with a two-atom vacancy are considered. Since the simulated nanotube is small, we do not consider vacancy defects with large size.

Figure 8 shows the failure stresses of nanocomposites compared with those of aluminum (Al) crystalline at various temperatures. High temperatures result in low strengths. It also can be seen that the pristine nanotube can enhance the strength of nanocomposites to 200% of that of Al crystalline. However, if the defected tubes with a two-atom vacancy are employed as inclusions, the enhancement of nanocomposite strength is only 25%, as illustrated in Fig. 8. For example, at the room temperature of 300 K, the strength of Al crystalline is 11.60 GPa. The strengths of pristine CNT/Al nanocomposite and defected CNT/Al nanocomposite are 22.7 and 14.5 GPa, respectively. The above phenomenon is due to the fact that defected nanotubes have much lower strengths than pristine nanotubes. A pristine (5,5) nanotube has the strength of 110.2 GPa at 300 K, but the strength of a (5,5) tube with a two-atom vacancy defect dramatically reduces to 62.1 Gpa. Consequently, the enhancement of vacancy-defected tubes as inclusions on the reinforcement of nanocomposites is not as significant as those of pristine tubes. It should be noted that only a two-atom vacancy defect is studied here. If a larger vacancy defect exists in the embedded nanotube, we believe that the effects of nanotube on reinforcement are less significant.

An interesting phenomenon can be observed in Fig. 9, which compares failure strains of Al crystalline and CNT/Al nanocomposites when the volume fraction of embedded nanotubes is 20%. It can be seen that pristine CNTs can

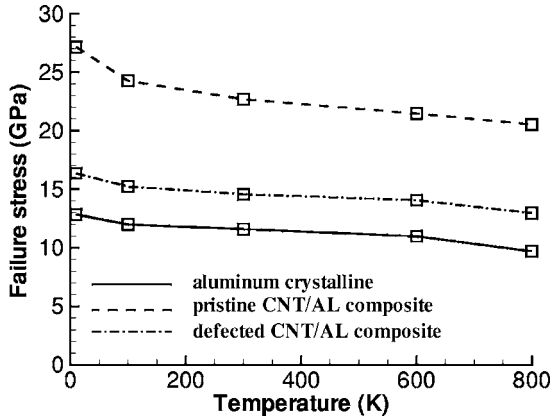

FIG. 8. Failure stresses of nanocomposites compared with those of aluminum crystalline.

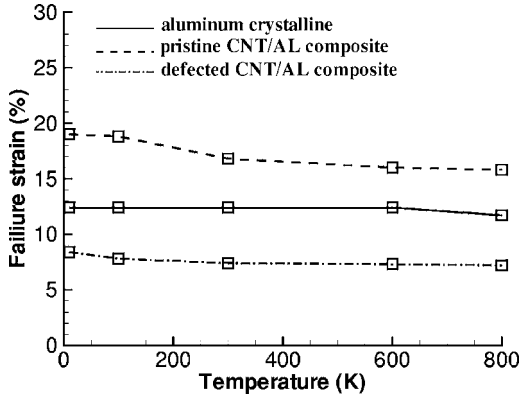

FIG. 9. Comparison of failure strains.

improve failure strains of nanocomposites but the defected CNTs decrease failure strains of nanocomposites even though the strengths are improved. Such phenomenon occurs because Al crystalline has a failure strain lower than a pristine CNT but higher than a defected tube. For instance, we investigate material failures at the room temperature of 300 K. Molecular dynamics simulation shows that the Al crystalline has the failure strain of 12.4%, and the failure strain of the pristine (5,5) nanotube is 19.6%. When the nanocomposite with the pristine (5,5) nanotube was under tension, we observed that the Al matrix fails first because its failure strain is smaller than that of the embedded nanotube. The nanotube bridges the cracks inside of the matrix, shown in Fig. 10, until it is broken, i.e., the nanocomposite fails. Consequently, the pristine nanotube reinforces the nanocomposite by increasing both the failure stress and the failure strain. On the other hand, the defected (5,5) nanotube with a two-atom vacancy fails at the 7.5% strain. When a defected tube is embedded in the nanocomposite, the nanotube will be broken first since it has smaller failure strain than the Al crystalline. Then, the nanocomposite fails quickly. We can conclude that the embedded defected nanotubes can increase the strength of CNT/Al nanocomposites but decrease their failure strains.

The above studies are based on the assumption that the volume fraction of embedded nanotubes is 20%. If various

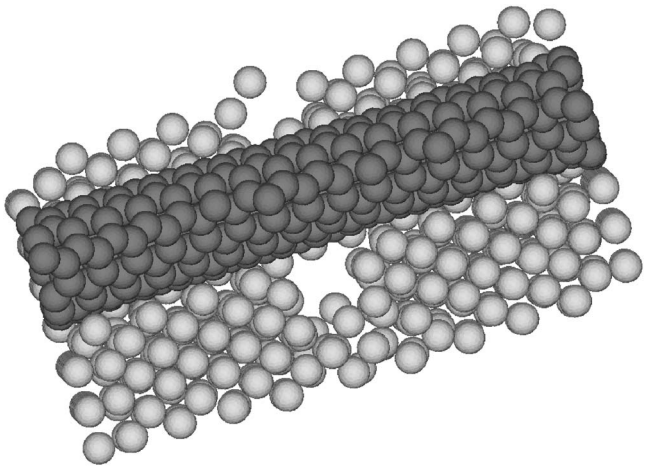

FIG. 10. A nanotube bridging the crack.

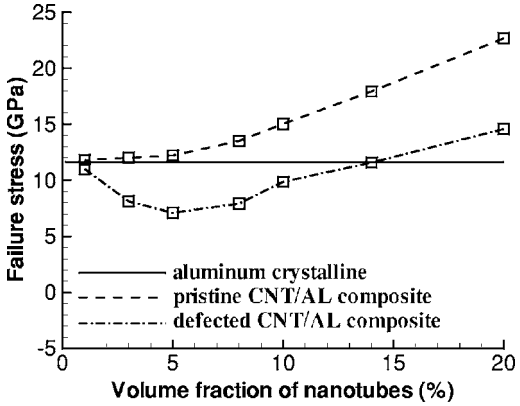

FIG. 11. Effects of volume fraction of embedded nanotubes on strength of CNT/Al composites.

volume fractions of nanotubes are considered, defected nanotubes will result in different characteristics of nanocomposites from those in which pristine nanotubes are embedded. The effects of volume fraction of embedded nanotubes on strength of CNT/Al nanocomposites are illustrated in Fig. 11. If pristine (5,5) nanotubes are embedded, lower strength of CNT/AL is calculated for a smaller volume fraction of nanotubes. The nanocomposite strength is similar to the strength of aluminum crystalline when the volume fraction is less than 5%. As well, an interesting phenomenon when defected (5,5) nanotubes are embedded is observed. When the volume fraction of defected nanotubes is less than 15%, it can be seen that nanotubes cannot reinforce but instead weaken CNT/Al composites. We think this phenomenon is due to the different roles of failure stress and strain of defected nanotubes in nanocomposites. As discussed above, failure stress of a two-vacancy defected (5,5) nanotube is larger than that of Al crystalline, while its failure strain is less than that of Al crystalline. Therefore, failure stress of the defected nanotube plays a role in reinforcing CNT/Al nanocomposites (i.e., increasing the strength of nanocomposites), while its failure strain plays a role in weakening the composites (i.e., decreasing the failure strain and in turn the strength of nanocomposites). When the volume fraction of a defected nanotube is 20% as studied above, failure stresses of nanotubes play a more important role than their failure strains. Consequently, defected nanotubes slightly reinforce the CNT/Al nanocomposites. At the volume fraction of 14%, effects from both failure stress and failure strain of the defected nanotube are balanced. Therefore, nanocomposites have the same strength as Al crystalline. If defected nanotubes with lower volume fractions are embedded, roles of their failure strains are more significant than those of their failure stresses. Then, such a phenomenon, in which nanocomposites are weakened by defected nanotubes as inclusions, is observed.

V. CONCLUSIONS

In this paper, we first studied the fracture of nanotubes containing vacancy defects. Compared with pristine nanotubes, strengths of vacancy-defected nanotubes are dramatically reduced according to the length of crack initiated via

the vacancy. We also found that temperature effects on the strength of vacancy-defected nanotubes are not as significant as those on the strength of pristine nanotubes. In addition, we employed CNT/Al nanocomposites to demonstrate whether vacancy-defected nanotubes can reinforce composite materials or not. Due to experimental observation, no chemical bonds exist at the CNT/Al interface. Several interesting phenomena were observed for defected CNT/Al composites other than pristine CNT/Al composites. At first, a critical volume fraction should be reached for vacancy-defected nanotubes to reinforce the aluminum matrix. For example, 14% is the critical volume fraction if (5,5) nanotubes with a two-atom vacancy defect are expected to increase the strength of CNT/Al nanocomposites. Second, although with a large volume fraction defected nanotubes can increase the failure stress, i.e., strength, of nanocomposites, the defected nanotubes reduce the failure strain of CNT/Al composites. We should point out that only the weak CNT/matrix interface is considered in this paper. Strong load transfer at the CNT/matrix interface may be achievable through functionalization of nanotubes. This will be our future research topic.

ACKNOWLEDGMENT

The authors acknowledge startup fund support from the College of Engineering and the Center for Computer-Aided Design (CCAD) at the University of Iowa.

[1] Q. Z. Zhao, M. B. Nardelli, and J. Bernholc, Phys. Rev. B **65**, 144105 (2002).
[2] E. W. Wong, P. E. Sheehan, and C. M. Lieber, Science **277**, 1971 (1997).
[3] S. Berber, Y. K. Kwon, and D. Tomanek, Phys. Rev. Lett. **84**, 4613 (2000).
[4] J. Hone, M. C. Liaguno, M. J. Biercuk, A. T. Johnson, B. Batlogg, Z. Benes, and J. E. Fischer, Appl. Phys. A: Mater. Sci. Process. **74**, 339 (2002).
[5] B. I. Yakobson, C. J. Brabec, and J. Bernholc, Phys. Rev. Lett. **76**, 2511 (1999).
[6] B. I. Yakobson, M. P. Campbell, C. J. Brabec, and J. Bernholc, Comput. Mater. Sci. **8**, 341 (1997).
[7] T. Belytschko, S. P. Xiao, G. C. Schatz, and R. Ruoff, Phys. Rev. B **65**, 235430 (2002).
[8] R. P. Raffaelle, W. Grande, and T. Gennett, Abstr. Pap. - Am. Chem. Soc. **225**, 284 (2003).
[9] C. Wei, D. Srivastava, and K. Cho, Nano Lett. **2**, 647 (2002).
[10] R. H. Baughman, A. A. Zakhidov, and W. A. de Heer, Science **297**, 787 (2002).
[11] M. F. Yu, O. Lourie, M. J. Dyer, K. Moloni, T. F. Kelly, and R. S. Ruoff, Science **287**, 637 (2000).
[12] T. Belytschko, S. Xiao and R. Ruoff, physics/0205090 (unpublished).
[13] S. L. Mielke, D. Troya, S. Zhang, J. Li, S. Xiao, R. Car, R. S. Ruoff, G. C. Schatz, and T. Belytschko, Chem. Phys. Lett. **390**, 413 (2004).
[14] D. B. Mawhinney, V. Naumenko, A. Kuznetsova, J. T. Yates, J. Liu, and R. E. Smalley, Chem. Phys. Lett. **324**, 213 (2000).
[15] M. Bockrath, W. Liang, D. Bozovic, J. H. Hafner, C. M. Lieber, M. Tinkham, and H. Park, Science **291**, 283 (2001).
[16] B. I. Yakobson, Appl. Phys. Lett. **72**, 918 (1998).
[17] H. Jiang, X. Q. Feng, Y. Huang, K. C. Hwang, and P. D. Wu, Comput. Methods Appl. Mech. Eng. **193**, 3419 (2004).
[18] F. Banhart, Rep. Prog. Phys. **62**, 1181 (1999).
[19] D. Qian, E. C. Dickey, R. Andrews, and T. Rantell, Appl. Phys. Lett. **76**, 2868 (2000).
[20] L. S. Schadler, S. C. Giannaris, and P. M. Ajayan, Appl. Phys. Lett. **73**, 3842 (1998).
[21] P. M. Ajavan, L. S. Schadler, C. Giannaris, and A. Rubio, Adv. Mater. (Weinheim, Ger.) **12**, 750 (2000).
[22] W. A. Curtin and N. Takeda, J. Compos. Mater. **32**, 2060 (1998).
[23] Z. Xia and W. A. Curtin, Acta Mater. **48**, 4879 (2000).
[24] M. P. O'Day and W. A. Curtin, J. Am. Ceram. Soc. **85**, 1553 (2002).
[25] Z. Xia, W. A. Curtin, and W. M. Peters, Acta Mater. **49**, 273 (2001).
[26] W. X. Chen, J. P. Tu, L. Y. Wang, H. Y. Gan, Z. D. Xu, and X. B. Zhang, Carbon **41**, 215 (2003).
[27] T. Kuzumaki, K. Miyazawa, H. Ichinose, and K. Ito, J. Mater. Res. **13**, 2445 (1998).
[28] W. G. Hoover, Phys. Rev. A **31**, 1695 (1985).
[29] Donald W. Brenner, Phys. Rev. B **42**, 9458 (1990).
[30] M. S. Daw and M. I. Baskes, Phys. Rev. B **29**, 6443 (1984).
[31] P. M. Agrawal, B. M. Rice, and D. L. Thompson, Surf. Sci. **515**, 21 (2002).
[32] T. Dumitrica, T. Belytschko, and B. I. Yakobson, J. Chem. Phys. **118**, 9485 (2003).